Modulation of COVID-19 Epidemiology by UV-B and –A Photons from the Sun

Authors:
Fabrizio Nicastro[1*], Giorgia Sironi[2], Elio Antonello[2], Andrea Bianco[2], Mara Biasin[3], John R. Brucato[4], Ilaria Ermolli[1], Giovanni Pareschi[2], Marta Salvati[5], Paolo Tozzi[4], Daria Trabattoni[3], Mario Clerici[6]

Affiliations:

1 Italian National Institute for Astrophysics (INAF) – Rome Astronomical Observatory, Rome, Italy
2 Italian National Institute for Astrophysics (INAF) – Brera Astronomical Observatory, Milano/Merate, Italy
3 Department of Biomedical and Clinical Sciences L. Sacco, University of Milano, Milano, Italy
4 Italian National Institute for Astrophysics (INAF) – Arcetri Astrophysical Observatory, Firenze, Italy
5 Regional Agency for Environmental Protection of Lombardia (ARPA Lombardia), Milano, Italy
6 Department of Pathophysiology and Transplantation, University of Milano and Don C. Gnocchi Foundation, IRCCS, Milano, Italy

Summary

It is well known that 200-290 nm ultraviolet photons (hereinafter UV-C radiation) photo-chemically interacts with DNA and RNA and are endowed with germicidal properties that are also effective on viruses (*1-8*). Fortunately, Solar UV-C photons of this wavelength are filtered out by the Ozone layer of the upper Atmosphere, at around 35 km (*9*). Softer UV photons from the Sun with wavelengths in the range 290-320 nm (UV-B) and 320-400 nm (UV-A), however, do reach the Earth's surface. The effect of these photons on Single- and Double-Stranded RNA/DNA viruses (*9-12*) and the possible role they play on the seasonality of epidemics (*13*), are nevertheless little studied and highly debated in alternative or complementarity to other environmental causes (*14-20*). Notably though, the effects of both direct and indirect radiation from the Sun needs to be considered in order to completely explain the effects of UV radiations in life processes (with e.g. the UV virucidal effect enhanced in combination to the concomitant process of water droplets depletion because of Solar heat).
Herein we present a number of concurring circumstantial evidence suggesting that the evolution and strength of the recent Severe Acute Respiratory Syndrome (SARS-Cov-2) pandemics (*21, 22*), might be have been modulated by the intensity of UV-B and UV-A Solar radiation hitting different regions of Earth during the diffusion of the outbreak between January and May 2020. Out findings, if confirmed by more in depth data analysis and modeling of the epidemics, which includes Solar modulation, could help in designing the social behaviors to be adopted depending on season and environmental conditions.

Coronavirus infections were shown to be influenced by seasonal factors including temperature and humidity (*23*). However, these factors have not been observed to modulate the geographical pandemics development of the ongoing SARS-CoV-2 infection (*24*). Yet, the available data on SARS-CoV-2 contagions show that the ongoing pandemic has a lower impact during summer time and in countries with a high solar illumination. This suggests that UV-B/A Solar photons may play a role in the evolution of this pandemic.

The optical-ultraviolet solar spectrum peaks at a wavelength of about 500 nm, but extends down to much more energetic photons of about 200 nm. Due to photo-absorption by the upper Ozone layer of the Earth's atmosphere, however, only photons with wavelengths longer than ~290 nm (those not sufficiently energetic to efficiently photo-excite an O_3 molecule and dissociate it into an O_2 + O), reach the Earth's surface (*25*). For a given exposure, the daily fluence (flux integrated over a daytime) on Earth of this UV radiation depends critically on Earth location (latitude) and time of the year and results in the potential of Solar UV-B/A photons to inactivate a virus in air (aerosol) or surfaces.

To evaluate this potential on the onset, diffusion and strength of the recent SARS-CoV-2 pandemics, in our analysis we use the action spectrum (i.e. the ratio of the virucidal dose of UV radiation at a given

wavelength to the lethal dose at 254 nm see Methods) compiled in 2005 by Lytle and Sagripanti (*12*), together with UV-B and –A solar radiation measurement estimates on Earth as a function of Earth's latitude and day of the year (taken from the Tropospheric Emission Monitoring Internet Service – TEMIS[1] – repository of Solar UV data (*26*): see Methods).

Figure 1 shows two world maps with superimposed a τ_0 intensity-gradient image, where τ_0 is the lethal-time in minutes needed to deliver the D_0(SARS-CoV-2)=3.1 J m^{-2} UV lethal dose inferred from the reference value for coronaviruses (*12*) and confirmed by preliminary measurements performed by our group at the University of Milan (see Methods, also for a discussion on the conservativeness of the assumptions made to estimate the τ_0). Data refers to 1 January 2020 (top panel) and 1 May 2020 (bottom panel; details in Figure's caption). On 1 January subtropical regions (latitude angle α<20 degrees) receive UV doses a factor of ~20 higher than temperate regions in the north hemisphere ($\alpha\approx$30-50 degrees), while the effect greatly mitigates in May and inverts in July.

TEMIS data are also used in Figure 2, where the five curves show the lethal-time τ_0, as a function of Earth's latitude, for the first four months and twenty days of 2020, as labeled in Figure (see Methods for further discussion). These curves clearly show that during the first three months of the considered period (January^{1st} – May^{20th}), UV-B/A solar photons on Earth's surface at latitudes $-60 < \alpha < -40$ degrees are sufficient to inactivate 63% of ss-RNA viruses within 4-to-35 minutes, depending on the exact latitude and time of the year. Between 0.33 and 14 hours are needed instead to obtain the same effect in the same period of the year, at latitudes comprise between α = 40–60 degrees north. The situation is almost reversed in April-May, when 0.33–8 hours are needed at $-60 < \alpha < -40$ degrees whereas 8-25 minutes are sufficient at α = 40–60 degrees north.

To investigate the effect of this radiation on the diffusion and strength of the SARS-CoV-2 pandemics, we collected COVID-19 data from the GitHub repository provided by the Coronavirus Resource Center of the John Hopkins University.[2]
Histograms in Figure 2 show the number of detected SARS-CoV-2 cases per thousand inhabitants and per Earth's latitude bins of $\Delta\alpha=5^0$, as of May 20th (see Figure's caption for details).

Strikingly, the number of SARS-Cov-2 cases cumulated over the period 22- January – 31 March at latitudes α>25 degrees north, greatly outnumber the number of cases registered in the remaining of the world. On the other hand, and offering further support to our hypothesis, very few or no cases developed in January – March at $\alpha < -20$ degrees, in the 16 countries sampled (including, some highly populated and with high density population areas, e.g. big cities in Australia, New Zealand, South Africa, Chile, Argentina and Zimbawe). Incidence data on SARS-CoV-2 infection shows that the vast majority of cases between January – March were observed at α>35 degrees, where about 100 countries are sampled. In the same period, incidence of infection, at tropical latitudes, where the majority of the sampled countries are present (about 150) was minimal, as only a modest number of cases were observed between January and April. It is important to underline that some of these tropical areas are highly populated and have high average cloud-coverage/day fraction from January through May (central and tropical south America, central Africa and south-east Asia), while the monsoon season starts in May in South India and extends rapidly to the north from May through September.

Results are summarized quantitatively in Figure 3, where the number of SARS-CoV-2 cases-per-thousand and per number of countries per Earth's latitude bin is shown to linearly correlate with the lethal-time τ_0 in log-log space (see Methods).

Figure 3 shows that the number of SARS-CoV-2 cases per thousand inhabitants and per number of Countries per Earth's latitude bin, with onset of the epidemics in the months of January, February, March and April 2020, correlates with the lethal-time τ_0. As expected, given the exponential growth of epidemics and the typical power-law shape of action spectra, this correlation is linear in the adopted log-log space.

---

[1] http://www.temis.nl
[2] https://github.com/CSSEGISandData/COVID-19

We did not attempt to correct the data for social-distancing measures (generally adopted more severely by northern Countries, compared to tropical or south Countries) or for tropical daily cloud-coverage (where present during the first four months of the year), which both certainly contribute significantly to the scatter visible in the data. Nonetheless, the correlation in Fig. 3 is statistically highly significant and extends over three orders of magnitudes in τ_0 and almost five orders of magnitude in number of SARS-CoV-2 cases. A simple linear-regression Pearson-test of these data-points, yields a null-probability of p=0.000415, corresponding to a Gaussian equivalent significance of 3.35σ. The correlation is also present when the number of SARS-Cov-2 cases-per-thousand is not normalized by the number of Countries in the latitude bin, but the statistical significance reduces to 3σ.

The histograms in Fig. 2 are only indicative of the total cumulated number of cases per country, but say nothing about the growth of the outbreak in each country from their onsets. Figure 4 allows us, instead, to evaluate the momentum of the SARS-Cov-2 epidemics (speed of diffusion times number of new daily case) in each of the 261 countries sampled (see details in Figure's caption). Interestingly, onset of the epidemics earlier than 10 March 2020 was only seen in Northern countries, when at these latitudes the minimum exposure needed by UV-B/A photons to inactivate 63% of the virus is longer than 20 minutes (black dotted curve).

Moreover, in Northern countries (black curves) the outbreaks proceeded at high rates for tens of days, reached peaks typically higher than a few hundreds and up to ten thousand new cases per day (i.e. high momentum, despite the severe measures of social distancing adopted by the majority of these countries) between end of March and mid April, and then started decreasing typically when the minimum UV-B/A virus- inactivation exposure is less than 10 minutes.

As expected by our model, in South- and Tropical-countries the onset of the outbreak was homogeneously distributed between the end of March through May (when typical UV-B/A virus-inactivation exposures are between 4-and-20 minutes: yellow and blue dotted curves), and after an initial fast growth the epidemics quickly slowed down, being limited to tens-to-hundreds new cases per day (low momentum).

There are a few interesting exception, both in the South and Tropical groups of countries. In the Tropical group, Brazil (where no restriction measures have been adopted till recently), contagions have developed at a high rate from mid March through beginning of April to then proceed constantly at a slower rate and reach about fifteen thousand new cases per day on 20 May 2020. The majority of these cases are now developing in the northern areas of the country, where humidity and cloud-coverage are higher. Peru follows a similar path, but the onset of the epidemics is in April.
In the South group, Chile, Argentina and South Africa after a long initial contained phase of the epidemics that saw no more than a few hundreds new cases per day (low momentum), SARS-CoV-2 contagions started spreading again towards the end of April (when needed UV-B/A lethal exposures are >20 minutes), and reached values of about 3000, 400 and 900 new cases per day, respectively on 20 May 2020 (increasing momentum).

The segregation by Earth's latitude of the curves of growth of Figure 4 can be well reproduced qualitatively by simulating the effect of the Sun with Monte-Carlo runs of simple diffusive model solutions, as detailed in Methods and shown in Figures 1 and 2 of the Extended Data (ED).

Taken together, the curves of growth of Figure 4, suggest that the epidemics efficiently develops in areas where typical UV-B/A virus-inactivation exposures are longer than about 20 minutes (but see Methods for the conservativeness of our assumptions on τ_0).
This value should be compared to the stability of SARS-CoV-2 on aerosol and surfaces. A recent study (*27*) shows that SARS-CoV-2 can survive in aerosols for longer than three hours and is even more stable on metallic and polymeric surfaces, where it can stay for up to several tens of hours. These results, combined with another recent research showing that the lifetime of speech droplets with relatively large size (> few micrometers) can be tens of minutes (*28*), suggest that SARS-CoV-2 may spread through aerosols (either directly, through inhalation, and/or indirectly, through evaporation of contaminated surfaces).

Our results suggest that Solar UV-A/B might have had a role in modulating the strength and diffusion of the SARS-CoV-2 epidemics, explaining the geographical and seasonal differences that characterize this disease. The also imply, if confirmed, that the UV flux received by our Sun in open areas may represent an important disinfection factor, able to significantly reduce the diffusion of the pandemics. This could help in designing new strategies of confinement of the epidemics that may provide better protection with less social costs (see e.g. (*28*)).

Acknowledgments

The work presented in this paper has been carried out in the context of the activities promoted by the Italian Government and in particular, by the Ministries of Health and of University and Research, against the COVID19 pandemic. Authors are grateful to INAF's President, Prof. N. D'Amico, for the support and for a critical reading of the manuscript. Authors are also grateful to Prof. A. Musarò, Dr. M. Elvis, and Dr. F. Fiore for critically reading the papers and providing useful comments and suggestions.

Authors' Contribution

All authors contributed equally to the discussion of the results and the writing of manuscript.

Conflict of Interest

Authors have no competing interest to disclose.

References

1. Kowalski W. Ultraviolet germicidal irradiation handbook: UVGI for air and surface disinfection (Springer Science & Business Media, 2010).
2. Rauth AM. The Physical State of Viral Nucleic Acid and the Sensitivity of Viruses to Ultraviolet. *Light Biophys J* 1965; **5**: 257–273.
3. Kesavan J, Sagripanti JL. Disinfection Of Airborne Organisms By Ultraviolet-C Radiation And Sunlight. Research and Technology Directorate, Edgewood Chemical Biological Center, U.S. Army, Aberdeen Proving Ground, Maryland 21010-5424 2012 ECBC-TR-1011.
4. Chang JC, Ossoff SF, Lobe DC, et al. UV Inactivation of Pathogenic and Indicator Microorganisms. *Appl. Env. Microb*. 1985; **49**: 1361-1365.
5. McDevitt JJ, Rudnick SN, Radonovich L. Aerosol susceptibility of influenza virus to UVC light. *Appl Environ Microbiol* 2012; **78**, 1666–1669.
6. Welch, D., Buonanno, M., Grilj, V. et al., Far-UVC light: A new tool to control the spread of airborne-mediated microbial diseases. *Scientific Reports* 2018; **8**, 2752.
7. Walker CM, Ko G. Effect of ultraviolet germicidal irradiation on viral aerosols. *Environ Sci Technol* 2007; **41**, 5460-5465.
8. Tseng CC, Li CS. Inactivation of Virus-Containing Aerosols by Ultraviolet Germicidal Irradiation. *Aerosol Science and Technology* 2005; **39**, 1136-1142.
9. Lubin D, Jensen EH. Effects of Clouds and Stratospheric Ozone Depletion on Ultraviolet Radiation Trends. *Nature* 1995; **377**, 710–713.
10. Jagger J. *Solar-UV Actions on Living Cells* (Praeger: New York, 1985).
11. Furusawa Y, Suzuki K, Sasaki M. Biological and physical dosimeter for monitoring solar UV-B light. *J Radiat Res 1990*; ***31***, 189–206.
12. Lytle DC, Sagripanti JL, Predicted Inactivation of Viruses of Relevance to Biodefense by Solar Radiation. *J Virol* 2005*;* **79**, 14244–14252.
13. Martinez ME, The calendar of epidemics: Seasonal cycles of infectious diseases. *PLoS Pathog* 2018*;* **14**, e1007327.
14. Hemmes JH, Winkler KC, Kool SM. Virus survival as a seasonal factor in influenza and poliomyelitis. *Nature 1960;* **188**, 430–431.
15. Sagripanti JL, Lytle CD. Inactivation of Influenza Virus by Solar Radiation. *Photochemistry and Photobiology* 2007*;* **83**, 1278–1282.
16. Nguyen MT, Silverman AI, Nelson KL, Sunlight Inactivation of MS2 Coliphage in the Absence of Photosensitizers: Modeling the Endogenous Inactivation Rate Using a Photoaction Spectrum. *Environmental Science and Technology* 2014; **48**, 3891−3898.

17. Weberand ThP, Stilianakis NI. A Note on the Inactivation of Influenza A Viruses By Solar Radiation, Relative Humidity and Temperature. *Photochemistry and Photobiology* 2008; **84**, 1601–1602.
18. de Arruda E(1), Hayden FG, McAuliffe JF, et al. Acute respiratory viral infections in ambulatory children in urban northeast Brazil. J Infect Dis 1991; **164**, 252–258.
19. Alonso WJ *et al.* Seasonality of influenza in Brazil: A traveling wave from the Amazon to the subtropics. *Am J Epidemiol* 2007*;* **165**, 1434–1442.
20. Patterson R. Why Pandemics Erupt, White Paper, April 2020 https://medium.com/@tallrobert/why-pandemics-erupt-e949a70878f8
21. Zhu N, Zhang D, Wang W, et al. A Novel Coronavirus from Patients with Pneumonia in China 2019. *New Engl J Med 2020*; **382**, 727-733.
22. Cobey S. Modeling infectious disease dynamics - The spread of the coronavirus SARS-CoV-2 has predictable features. *Science 2020;* **368**, 713.
23. Monto AS et al. Coronavirus Occurrence and Transmission Over 8 Years in the HIVE Cohort of Households in Michigan. *The Journal of Infectious Diseases* 2020; jiaa161.
24. Baker RE, Yang W, Vecchi GA. Susceptible supply limits the role of climate in the early SARS-CoV-2 pandemic. *Science* 2020; 10.1126/science.
25. Nelson KL, Boehm AB, Davies-Colley RJ *et al.* Sunlight-mediated inactivation of health-relevant microorganisms in water: a review of mechanisms and modeling approaches. *Environmental Science: Processes & Impacts* 2018; **20**, 1089-1122.
26. Zempila MM, van Geffen JHGM, Taylor M, et al. TEMIS UV product validation using NILU-UV ground-based measurements in Thessaloniki, Greece. Atmos *Chem Phys* 2017; **17**, 7157–7174.
27. van Doremalen N, Bushmaker T, Morris D, et al. Aerosol and Surface Stability of SARS-CoV-2 as Compared with SARS-CoV-1. *N Engl J Med* 2020*;* **382**, 1564-1567.
28. Stadnytskyi V, Anfinrud Ph, Bax CE, Bax A. The airborne lifetime of small speech droplets and their potential importance in SARS-CoV-2 transmission. *PNAS* 2020; 2006874117.
29. Ratnesar-Shumate S, Williams G, Green B, *et al*. Simulated Sunlight Rapidly Inactivates SARS-CoV-2 on Surfaces. *The Journal of Infectious Diseases* 2020; jiaa274 https://doi.org/10.1093/infdis/jiaa274.
30. Mousavizadeh L, Ghasemi S. Genotype and phenotype of COVID-19: Their roles in pathogenesis. *Journal of Microbiology, Immunology and Infection*; 2020, in press
31. Rabaan AA et al. SARS-CoV-2, SARS-CoV, and MERS-CoV: a comparative overview. *Le Infezioni in Medicina*, **2**, 174-184 (2020).
32. Weiss W, Horzinek MC. Resistance of Berne Virus to Physical and Chemical treatment. *Veterinary Microbiology* 1986; **11**, 41-49.
33. Kowalski WJ, Bahnfleth WP, Hernandez MT. A Genomic Model for the Prediction of Ultraviolet Inactivation Rate Constants for RNA and DNA Viruses. *IUVA News*, June 2009.
34. K. R. Wigginton, T. Kohn, Virus disinfection mechanisms: the role of virus composition, structure, and function. *Current Opinion in Virology* 2012, **2** 84–89 (2012)
35. Nelson KL, Boehm AB, Davies-Colley RJ et al., Sunlight-mediated inactivation of health-relevant microorganisms in water: a review of mechanisms and modeling approaches. *Environmental Science: Processes & Impacts* 2018; **20**, 1089-1122.
36. Madronich S. The Atmosphere and UV-B Radiation at Ground Level, in *Environmental UV Photobiology*, A. R. Young, J. Moan, L. O. Björn, and W. Nultsch, Eds. Boston (MA: Springer US, 1993), pp. 1–39.
37. Molina MJ, Rowland FS. Stratospheric sink for chlorofluoromethanes: chlorine atom-catalysed destruction of ozone. *Nature* 1974*;* **249**, 810-812.

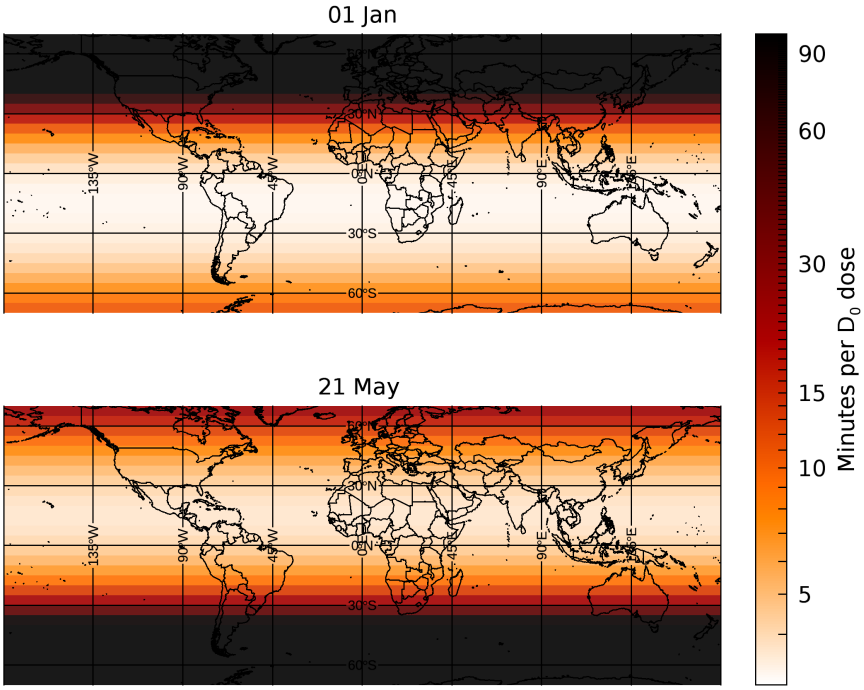

Figure 1 Exposing the World to UV Light.
World maps with superimposed a lethal-time intensity-gradient image, as derived from Temis UV-B/A data. Data refers to 1 January 2020 (top panel) and 1 May 2020 (bottom panel). On 1 January subtropical regions (latitude angle $\alpha<20$ degrees) receive UV doses a factor of 5 higher than temperate regions in the north hemisphere ($\alpha\approx30$-50 degrees), while the effect greatly mitigates in May and inverts in July.

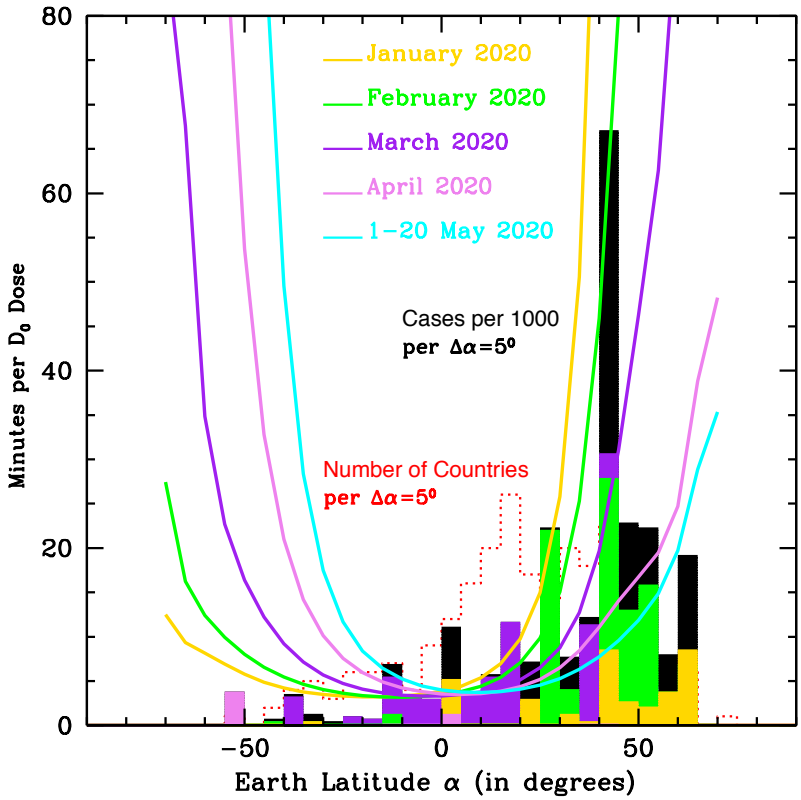

Figure 2 Effects of the Sun on SARS-CoV-2.
The five curves show the UV-B/A lethal-time τ_0, as a function of Earth's latitude, for the first four months and twenty days of 2020, as labeled. The black filled histogram shows the number of detected SARS-CoV-2 cases per thousand inhabitants and per Earth's latitude bins of $\Delta\alpha=5^0$, as of 20 May 2020, in the 261 Countries (or regions for Australia, China and the United Kingdom) for which continuous coverage from 22 January 2020 through 20 May 2020 is available. Color-filled histograms superimposed to the black histogram, are the number of SARS-CoV-2 cases color-coded according to the actual onset of the epidemics in each Country: from January 2020 (yellow) through February (green), March (purple) and April (violet). Finally, The red, dotted, empty histogram shows the distribution of sampled countries per $\Delta\alpha=5^0$ bins.

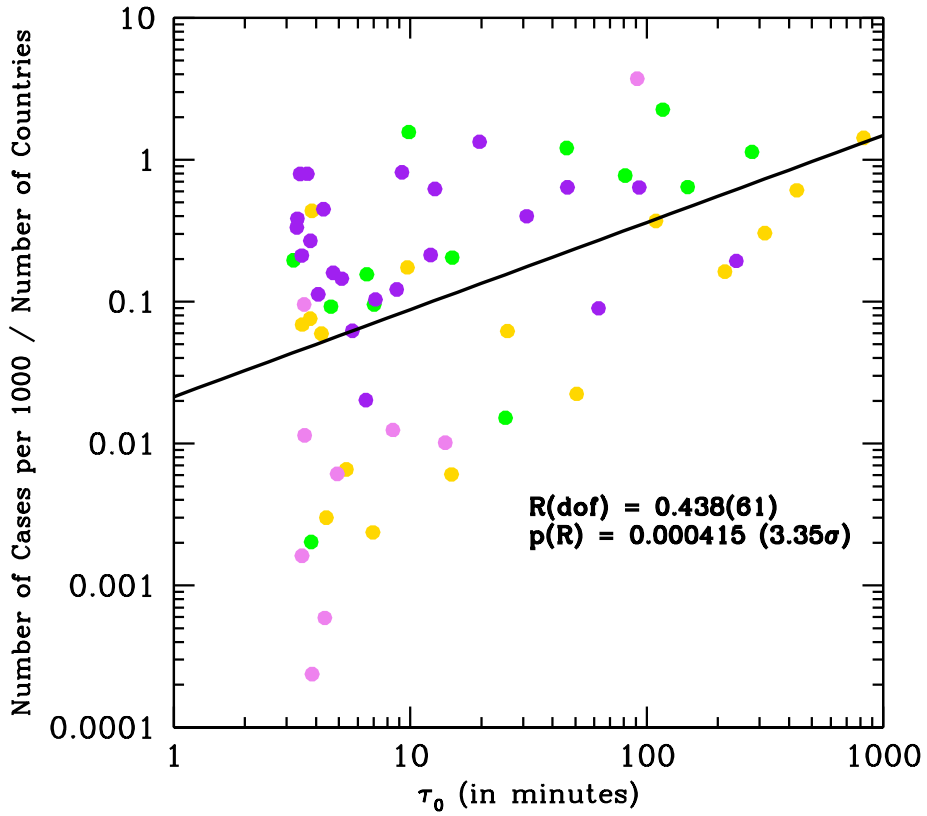

Figure 3 Correlation of Number of SARS-CoV-2 Cases and Virus Lethal-Time.
Number of total SARS-CoV-2 case-per-thousand per $\Delta\alpha$=5 degrees bin of Earth's latitude and per number of Countries per latitude's bin, cumulated as of May 20th in the 261 sampled Countries, versus the lethal-time τ_0 as derived from the curves of Fig. 2. Colors indicate the month of onset of the epidemics: January (gold), February (green), March (purple) and April (violet).

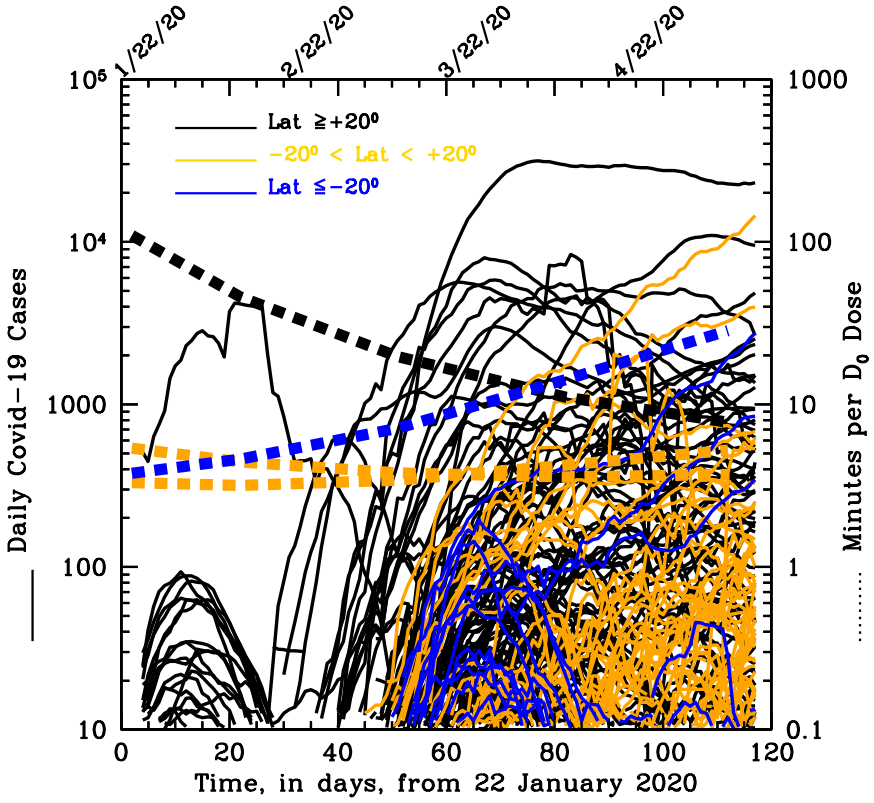

Figure 4 Momentum of the SARS-CoV-2 Pandemics.
Compilation of the curves of growth of the daily SARS-CoV-2 new cases in each of the 261 countries sampled. The product between the speed of diffusion and the number of cases cumulated during diffusion is indicative of the Momentum of the epidemics in each country. Curves are color-coded according to three broad latitude regions, the North (α>20 degrees, black curves), the South (α<-20 degrees; blue curves) and the Tropical strip (-20 < α < 20 degrees; orange curves). The four additional dotted curves indicate the exposures needed at α=+40 degrees (black), α=-10 and +10 degrees (orange) and α=-35 degrees (where most of the South countries are located; blue).

Methods

UV-C Lethal Dose for SARS-CoV-2

In 2005, Lytle and Sagripanti *(12)* reviewed several experimental studies of inactivation of viruses[3] by UV light exposure and reported the mean lethal dose at 254 nm (the UV wavelength at which the maximum inactivation of virus takes place) in terms of fluence (J m^{-2}) needed to inactivate 63% of the virus (D_0 hereinafter).

They concluded that the product between the mean lethal dose at 254 nm D_0 and the size of the genoma (Size-normalized Sensitivity - SnS) is approximately constant. This means that larger doses of UV radiation are needed to produce the same fraction of inactive viruses with smaller sizes. For the SARS-CoV-2, with a measured genome-size of 29.8-29.9 kb *(30, 31),* we assume the experimentally-measured lethal dose D_0=3.1 J m^{-2} at 254-nm as reported by Lytle and Sagripanti *(12)* and measured by M. Weiss and M.C. Horzinek *(32)* for the Berne coronavirus, which has genome size of 28 kb similar to that of SARS-COV-2. Other authors suggested alternative models which consider specific sequences of the nucleic acid (33), however measurements in aerosol for other coronaviruses and ss-RNA viruses *(5, 6, 7, 8)* obtained results in agreement with Lytle and Sagripanti *(12)*. Moreover, we anticipate that a range of values D_0=2.9–3.1 J m^{-2} at 254-nm, fully consistent with the value reported by *(12)* for the Berne coronavirus, has been recently measured by our group for the COVID-19 at the Laboratories of the University of Milan (these measurements are the subject of a forthcoming paper).

Solar Radiation and Microorganisms

The mechanisms through which UV radiation from the Sun acts on viruses and, in general, microorganisms are both endogenous and exogenous and depend on the exact wavelength of the photons. For viruses, the direct endogenous mechanism is the most important, and consists in direct absorption of the UV photon by the chromophore embedded in the virus, as the nucleic acid or protein (*34*). This process is known to decrease in efficiency going from UV-C to UV-B and is not active in the UV-A, where only the exogenous mechanism is effective (*35*).

UV strongly interacts with gaseous and aerosol pollutants in the air affecting the amount of UV spectrum reaching the Earth surface. Nitrogen and Sulphur oxides together with Ozone strongly absorb UV light with efficiency increasing from UV-A to UV-B *(36).* In addition, scattering of light by particles and aerosols is proportional to their concentration and highly polluted areas show again a UV reduction effect that goes in the same direction of molecular absorption.

Solar UV Data

In our analysis, we use Solar UV data made available by the Tropospheric Emission Monitoring Internet Service (TEMIS) archive[4].

TEMIS is part of the Data User Programme of the European Space Agency (ESA), a web-based service that stores, since 2002, calibrated atmospheric data from Earth-observation satellite. TEMIS data products include measurements of ozone and other constituents (e.g. NO_2, CH_4, CO_2, etc.), cloud coverage, and estimates of the UV solar flux at the Earth's surface. The latter are obtained with state-of-the-art models exploiting the above satellite data. It should be noted a depletion of the Ozone stratospheric layer has been observed during the last few decades due to interaction with Cloro-Fluoro-Carbon (CFC) gas emitted in industrial activities, with consequent increase of the atmosphere transparences to UV light *(37).*

UV-B/A Action Spectrum

Lytle and Sagripanti *(12)* estimated SnS in the 280-320nm wavelength range for a variety of viruses with known genome compositions and sizes by compiling measurements obtained at longer wavelengths longer and normalizing them to 254 nm. The final product is the UV-B/A action spectrum, defined as the ratio of the lethal dose at a given wavelength to the dose at 254 nm.

---

[3] Including viruses with single- and double-stranded DNA/RNA and ee-stranded genoma

[4] http://www.temis.nl

TEMIS UV products include integrated UV doses [in kJ/m^2] weighted for different action spectra, normalized at 300 nm. In this study we use TEMIS data folded through the unshielded-DNA damage action spectrum and renormalized to 254 nm. This renormalization brings the two action spectra TEMIS DNA and Lytle and Sagripanti single- and double-stranded RNA/DNA (*12*) to match in the common 250-320 nm wavelength range, and yields to the virucidal UV-B/A flux F_{vir}, in J m^{-2} day^{-1} used in our analysis.

Lethal Exposure as a function of Earth's latitude and Time of the year

To obtain the curves of exposure needed to irradiate the lethal dose as a function of Earth's latitude, we considered the whole TEMIS data set (259 locations around the world) for year 2019 and 2020 and interpolated on a regular latitude grid of 5 degrees. We conservatively considered only the 20% of the Solar flux F_{vir} released in the one hour interval centred around local noon and computed the virucidal UV flux per minute when the Sun is close to its daily maximum elevation. The lethal exposure, in minutes, is thus given by:

$$\tau_0 = \tau_{0,noon} = \frac{D_0}{0.2 * F_{vir}} * 60$$

Our Conservative Assumptions

All the approximations we used to compute τ_0 are conservative:

i) the F_{vir} vs latitude dependence was obtained by excluding locations with altitude > 400 m, where F_{vir} values are higher because of the thinner atmosphere column.

ii) the adopted fraction of 0.2 F_{vir} is the minimum value obtained by simulating the UV Index[5] for a given instantaneous zenith angle (as a function of latitude and time of the year) and computing the fractional dose released in a one-hour time interval centered on the local noon: for comparison, the mean observed attenuation factor is 0.34 F_{vir}. Properly distributing the remaining 80% of the daily solar flux in time as a function of latitude and time of the year, would lower the threshold of the minimum lethal exposure.

iii) TEMIS data on broad global scale are only available for clear sky. For Europe and few locations of central America and the south hemisphere cloud correction is available. The difference between cloud corrected and clear sky data show high frequency fluctuations due to weather superimposed to a low frequency seasonality effect (winter/summer modulation in temperate areas and rain/dray seasons in the tropical areas). Considering cloud-coverage would then amplify (in both directions) the observed latitude effect of Solar virucidal power.

iv) aerosols are the main responsible for local F_{vir} absorption and scattering and may vary greatly from location to location on Earth. TEMIS data account for this effect by reducing F_{vir} via a flat mean attenuation factor of 0.3. Experiments made on ground showed actual doses up to a factor 2 higher than those reported by TEMIS *(5)*, implying that the adopted flat 0.3 factor is highly conservative[6].

SARS-CoV-2 Pandemics Data

We collect SARS-CoV-2 data pandemics from the on-line GitHub repository provided by the Coronavirus Resource Center of the John Hopkins University (CRC-JHU)[7]. CRC-JHU global data are updated daily and cover, currently, the course of epidemics in 261 different world countries (and regions for Australia, Canada, United Kingdom and China), by providing the daily cumulated numbers of Confirmed SARS-CoV-2 cases, Deaths and Healings. We use CRC-JHU data run from 22 January 2020 (recorded start of the epidemics in China) through 20 May 2020.

---

[5] http://www.temis.nl/uvradiation/product/papers/WR2016-01.pdf

[6] Local aerosol measurements would be incredibly interesting to study infection diffusion in polluted areas but this would require specific data per targeted area and are beyond the scope of this analysis.

[7] https://github.com/CSSEGISandData/COVID-19

The black and color-filled histograms of Figure 2 are produced by grouping CRC-JHU global data of confirmed SARS-CoV-2 cases as of 20 May 2020, in Earth's latitude bins of $\Delta\alpha$=5 degrees, independently on the Earth's longitude of the sampled Countries.

The doted red histogram of Figure 2, shows the number of Countries per bin.

Black (North Countries), orange (Countries in the Tropical strips) and blue (South Countries) curves in Figure 4, are the curves of growth of the daily new confirmed SARS-CoV-2 cases, from the start of epidemics in each Country through May 20th. These curves are derived by first differentiating the cumulative curve of growths provided by CRC-JHU and then operating a non-weighted 7-day moving average on the data, to smooth non-Poissonian daily fluctuations (systematics).

Modeling the Earth's latitude Segregation of SARS-CoV-2 Cases with Simulations

The segregation by Earth's latitude of the SARS-CoV-2 curves of growth of Figure 3 can be well reproduced qualitatively by simulating the effect of the Sun with Monte-Carlo simulations of simple diffusive model solutions.

Figure 1 of the ED shows a run of such simulations. Simulations are run for 261 countries with latitudes and populations distributed randomly and uniformly accordingly to the three latitude groups in the observed SARS-CoV-2 pandemics data (100 North Countries: black curves; 145 Tropical Countries: orange curves; 16 South Countries: blue curves). Each curve represent the daily number of infections for a given Country and is the solution of a simple diffusive SIRD-like (Susceptible, Infected, Recovered, Deaths) model, where epidemics starts at a time T_{Start}, lockdown measures are taken at T_{LD} and reopening starts at T_{Open}. T_{Start}, T_{LD} and T_{Open} and randomly and uniformly distributed between the intervals labeled in the two panels of Fig 1 ED, as are the halving and doubling times of the reproductive number R_t, before lockdown and reopening, respectively. Lockdowns and re-openings are both modeled with exponential functions that act as attenuating and amplifying factors, respectively, of the daily probability of contacts between individuals, with halving and doubling times $T_{LD}^{1/2}$ and $T_{Open}^{1/2}$.

The two panels of Fig.1 ED differ only for the absence (top panel) or presence (bottom panel) of the Solar effect. The Solar effect is introduced as a daily piston, modeled as Gaussian functions which deliver 20% of the UV-B/A Solar flux observed between 1 January 2020 and 20 May 2020 (TEMIS data of Figure 2-4), with a standard deviation of 5 hours centered on local noon and peak-intensity inversely proportional to the lethal-time τ_0 (Figure 2 ED).

Segregation (by over an order) in Earth's latitude of the simulated daily SARS-CoV-2 infections, similar to that observed in real data (Fig. 3), can only be obtained by switching the Sun on (Fig. 1 ED, bottom panel).

Figures' Production

Figure 1 is produced via scripts written by us in the IDL scripting language.[8]

Figure 2–4 and Fig. 1–2 in the Extended Data, are produced via scripts written by us in the scripting language Supermongo[9].

[8] https://www.harrisgeospatial.com/Software-Technology/IDL

[9] https://www.astro.princeton.edu/~rhl/sm/sm.html